Applied Catalysis B: Environmental 163 (2015) 459–466

Contents lists available at ScienceDirect

Applied Catalysis B: Environmental

journal homepage: www.elsevier.com/locate/apcatb

Monopersulfate oxidation of 2,4,6-tribromophenol using an iron(III)-tetrakis(*p*-sulfonatephenyl)porphyrin catalyst supported on an ionic liquid functionalized Fe_3O_4 coated with silica

Qianqian Zhu [a], Shohei Maeno [a], Masahide Sasaki [b], Takafumi Miyamoto [a], Masami Fukushima [a,*]

[a] *Laboratory of Chemical Resources, Division of Sustainable Resources Engineering, Faculty of Engineering, Hokkaido University, Sapporo 060-6828, Japan*
[b] *National Institute of Advanced Industrial Science and Technology (AIST), 2-17-2-1 Tsukisamu-Higashi, Toyohira-ku, Sapporo 062-8517, Japan*

ARTICLE INFO

Article history:
Received 23 May 2014
Received in revised form 30 July 2014
Accepted 10 August 2014
Available online 27 August 2014

Keywords:
Fe_3O_4
Ionic liquid
Iron(III)-porphyrin
2,4,6-Tribromophenol
Humic acid

ABSTRACT

Iron(III)-tetrakis(*p*-sulfonatephenyl)porphyrin (FeTPPS), immobilized on ionic liquid (IL) functionalized Fe_3O_4, was used as a powerful catalyst for degrading TrBP. The prepared Fe_3O_4@SiO_2-IL-FeTPPS catalyst was characterized by SEM, TEM, TEM-EDX, XRD and FT-IR. The percent degradation of TrBP was calculated based on the initial and remained concentrations of TrBP, as determined by high performance liquid chromatography. The amount of Br^- released via the debromination was also determined by ion chromatography. The Fe_3O_4@SiO_2-IL-FeTPPS showed a high catalytic activity and 200 μM of TrBP was efficiently degraded at pH 6 using 500 μM $KHSO_5$, even in the presence of 86 mg L^{-1} humic acid, which is known as a major concomitant in waste waters. In addition, the degraded TrBP had undergone more than 50% mineralization, while 30% of mineralization was found for Fe_3O_4 alone as a control. The Fe_3O_4@SiO_2-IL-FeTPPS catalyst had a high catalytic activity for the degradation of TrBP, and the IL modified surface played a key role in restoring the homogeneous catalytic efficiency of the supported FeTPPS.

1. Introduction

Brominated flame retardants (BFRs) are one of the most frequently used and the largest group of commercial flame retardants currently on the market, due to their low cost and high performance [1]. 2,4,6-Tribromophenol (TrBP), a widely produced brominated phenol, is mainly used as an intermediate in preparing flame retardants in the electronics manufacturing industry, and is employed in production lines of electronic devices, such as televisions, computers and other household items. In addition, TrBP has been used as a fungicide, wood preservative, and this may lead to the accumulation of TrBP in soil and wood wastes [2]. The production volume of TrBP has been estimated to be approximately 2500 tons/year in Japan and 9500 tons/year worldwide in 2001 [3]. In 1998, the Environmental Protection Agency in the USA incorporated TrBP into its list of hazardous wastes [4]. Resent reports show that TrBP functions as an endocrine disruptor, interacting with thyroid hormone-binding transport proteins [2,5]. Wastes that contain TrBP are typically disposed into landfills. However, bromophenols such as TrBP are eluted into leachates via hydrophobic interactions with humic acids (HAs) in the landfills [6,7]. Because this may result in pollution of the aquatic environments, it is recommended that TrBP in landfill leachates should be degraded and detoxified.

Iron(III)-porphyrins, which mimic the active center of oxidative enzymes, have attracted much attention due to their high catalytic activity for the oxidation of halogenated phenols [8–21]. In homogenous catalytic systems, oxidative degradation in the presence of oxygen donors, such as $KHSO_5$ and H_2O_2, suffers from disadvantages such as deactivation as the result of the self-degradation of iron(III)-porphyrins [8,17,22], and the fact that they are not recyclable. To circumvent such problems, iron(III)-porphyrin catalysts are supported on solids, such as SiO_2 [13,14,19,20,9], mesoporous silica [12], polymers [20] and ion-exchange resins [11,23] to suppress self-degradation and enhance their recyclability. However, the catalytic activities (e.g., turnover frequency (TOF) and mineralization) of such complexes have not been correspondingly increased because of mass transfer limitations, the leaching of catalysts from the solid support, coverage of substrates and/or byproducts and competitive inhibition by other contaminants, such as HAs, in leachates [12–14]. In terms of catalytic activities, homogeneous catalytic systems are more advantageous than heterogeneous systems. For example,

* Corresponding author. Tel.: +81 11 706 6304; fax: +81 11 706 6304.
E-mail address: m-fukush@eng.hokudai.ac.jp (M. Fukushima).

http://dx.doi.org/10.1016/j.apcatb.2014.08.035
0926-3373/

homogeneous iron(III)-porphyrin catalysts that are incorporated into polyetectrolytes can be used to mineralize chlorophenols [8,21]. To overcome the disadvantages associated with heterogeneous catalysts, "liquid phase" methodologies have been introduced into solid catalysts in attempts to "restore" homogeneous catalytic conditions. For this purpose, ionic liquids (ILs) can be used as mobile and versatile "carriers" [24–28]. Supported-IL-phase (SILP) catalysts have recently been reported to be an alternative approach for the development of novel heterogeneous catalysts with advantages in facilitating separation workup and "restoring" homogeneous catalytic efficiency [29–31]. Among the numerous solid supports that have been applied to SILP catalysts, magnetite (Fe_3O_4) has attached considerable attention due to the capability of magnetic separation [32], and this is advantageous in practical use of such catalysts. In the present study, the IL was covalently anchored on the surface of Fe_3O_4 coated with silica and an iron(III)-tetrakis(*p*-sulfonatephenyl)porphyrin (FeTPPS) was introduced via the formation of an ion-pair by electrostatic interactions. The synthesized Fe_3O_4@SiO_2-IL-FeTPPS catalyst was characterized, and its catalytic activities were evaluated with respect to the oxidation of TrBP (degradation kinetics, inhibition by HA and mineralization).

2. Materials and methods

2.1. Materials

The soil HA sample used in this study was extracted from a Shinshinotsu peat soil, as described in a previous report [33]. The FeTPPS was synthesized by a previously reported method [34]. $FeCl_3$, TrBP, ethylene glycol, CH_3COONa, 3-chloropropyltrimethoxysilane (CPTMS), 1-methylimidazole and tetraethyl orthosilicate (TEOS) were purchased from Tokyo Chemical Industry. 2,6-Dibromo-*p*-benzoquinone (DBQ) was synthesized according to a procedure reported by Shigetatsu et al. [11]. Potassium monopersulfate ($KHSO_5$) was obtained as a triple salt, $2KHSO_5{\bullet}KHSO_4{\bullet}K_2SO_4$ (Merck). 5,5-Dimethyl-1-pyrroline-*N*-oxide (DMPO, 99%) was purchased from Labotec.

2.2. Synthesis of Fe_3O_4@SiO_2-IL-FeTPPS

The synthesis of the Fe_3O_4@SiO_2-IL-FeTPPS catalyst is summarized in Scheme 1.

2.2.1. Synthesis of Fe_3O_4

The Fe_3O_4 was synthesized through a hydrothermal reaction according to the procedures reported by Zhang et al. [32] with minor modifications. Briefly, $FeCl_3$ (0.8 g) was dissolved in ethylene glycol (40 mL) to form a clear solution under magnetic stirring. CH_3COONa (2.7 g) and polyethylene glycol (1.0 g) were then added to the solution and the resulting solution was stirred vigorously for 30 min and then sealed in a Teflon-lined stainless-steel autoclave (50-mL capacity). The autoclave was heated to 200 °C and maintained at that temperature for 8 h. After cooling to room temperature, the black-colored products were washed several times with water, ethanol and then dried in vacuo at room temperature.

2.2.2. Synthesis of IL functionalized Fe_3O_4

A 0.10 g portion of Fe_3O_4 particles (~300 nm in diameter) was treated with a 0.01 M HCl aqueous solution (50 mL) by ultrasonic irradiation. After treating for 10 min, the Fe_3O_4 particles were separated using a magnet and washed with ultrapure water, and then homogeneously dispersed in a mixture of ethanol (80 mL), ultrapure water (20 mL) and a concentrated aqueous ammonia solution (1.0 mL, 28 wt.%), followed by the addition of TEOS (0.03 g, 0.144 mmol). After stirring for 6 h at room temperature, the silica coated (Fe_3O_4@SiO_2) microspheres were separated, washed with ethanol, water, and then dried in vacuo. The prepared Fe_3O_4@SiO_2 (0.1 g) was redispersed in 80 mL ethanol containing concentrated ammonia aqueous (1.00 mL, 28 wt.%) by ultrasonication. The mixed solution was homogenized by mechanical stirring for 0.5 h to form a uniform dispersion. The IL (1-methyl-3-(trimethoxysilylpropyl)-imidazolium chloride) was then synthesized according to a previous report [35], and 0.1 g of the prepared IL was then added dropwise to the dispersion with continuous stirring. After stirring for 24 h, the product was collected with a magnet, washed several times with ethanol and water. Finally, the IL coated Fe_3O_4 (Fe_3O_4@SiO_2-IL) was dried at room temperature in vacuo.

2.2.3. Incorporation of FeTPPS into the IL functionalized Fe_3O_4

The Fe_3O_4@SiO_2-IL (0.6 g) was dispersed in 30 mL of a FeTPPS aqueous solution (3 mM) followed by shaking in an incubator at 25 °C for 42 h. After the reaction, the product was collected with a magnet and washed repeatedly with ultra-pure water until no Q-band for FeTPPS at 529 nm was detected in UV–vis absorption spectra. The final product, Fe_3O_4@SiO_2-IL-FeTPPS, was dried at room temperature in vacuo for 24 h.

2.3. Characterization of the synthesized catalyst

The loading amount of FeTPPS into the Fe_3O_4@SiO_2-IL-FeTPPS catalyst was estimated using UV–vis absorption spectroscopy on a V-650 iRM type spectrophotometer (Japan Spectroscopic Co. Ltd.). FT-IR spectra of the Fe_3O_4, Fe_3O_4@SiO_2, Fe_3O_4@SiO_2-IL and Fe_3O_4@SiO_2-IL-FeTPPS samples were collected using a FT/IR 600-type spectrophotometer (Japan Spectroscopic Co. Ltd.). Spectra were recorded between 4000 and 400 cm^{-1} at a resolution of 2 cm^{-1}, using a KBr disk. X-ray diffraction (XRD) patterns were collected using a RINT 2200 X-ray analyzer (Rigaku) with Cu Kα radiation. Transmission electron microscopy (TEM) and transmission electron microscopy-energy dispersive X-ray (TEM-EDX) measurements were carried out on a JEM-2100F instrument (JEOL) at an accelerating voltage of 200 kV. Scanning electron microscopy (SEM) images were obtained with a JEOL JSM-6501L instrument (JEOL). The zeta potential and particle size of the samples were recorded on an ELSZ-1000 type Zeta-potential & Particle Size Analyzer (Otsuka Electronics Co. Ltd). The oxidation-reduction potential (ORP) of the solutions was measured using an ORP electrode (PST-2729C (5), DKK-TOA Co. Ltd) connecting to a pH meter (HM-31P, DKK-TOA Co. Ltd).

2.4. Assay for TrBP degradation

A 20 mL aliquot of a 0.02 M phosphate buffer (pH 4–8) was placed in a 100-mL Erlenmeyer flask. A 400 μL aliquot of 0.01 M TrBP in acetonitrile and 20 mg of catalyst were then added to the buffer. A 100 μL aliquot of 0.1 M aqueous $KHSO_5$ was added, and the flask was then allowed to shake at 25 °C in an incubator. After the reaction, the concentrations of the remaining TrBP and a major degradation intermediate, DBQ, were measured by a standard method using HPLC with a UV detector. Separation was accomplished with a COSMOSIL $5C_{18}$-AR-II column (4.6 × 250 nm). The mobile phase was a mixture of methanol and water (68:32 in volume), acidified with aqueous 0.08% H_3PO_4. The flow rate was set at 1.0 mL min^{-1}, and the detection wavelength was at 290 nm. The released Br^- was analyzed by ion chromatography (ICS-90 type, Dionex). The mobile phase was a solution of 2.7 mM Na_2CO_3 and 0.3 mM $NaHCO_3$, and the flow rate was set at 1.5 mL min^{-1}. Electron spin resonance (ESR) spectra were recorded at room temperature using a quartz flat cell on a JEOL JES-TE300 ESR Spectrometer under the following conditions: microwave power 10 mW; microwave frequency 9.42 GHz; magnetic field 335 mT;

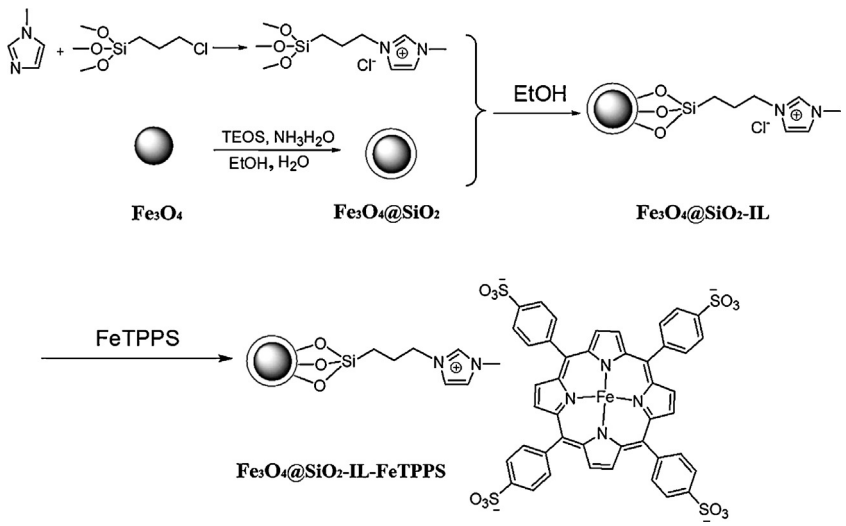

Scheme 1. Synthesis of the Fe_3O_4@SiO_2-IL-FeTPPS catalyst.

field amplitude ± 5 mT; modulation amplitude 0.079 mT; modulation width 20 μT; sweep time 2 min; and the time constant was 0.03 s. The Fe in the aqueous phase of the reaction mixture was determined by ICP-AES (ICPE9000, Shimadzu).

3. Results and discussion

3.1. Characterization of Fe_3O_4 and Fe_3O_4@SiO_2-IL-FeTPPS

The amount of loaded FeTPPS in the Fe_3O_4@SiO_2-IL was calculated by subtracting the absorbance of the filtrate at 393 nm after shaking with the mixture of aqueous FeTPPS and Fe_3O_4@SiO_2-IL from the original FeTPPS solution. The loading amount of FeTPPS in the Fe_3O_4@SiO_2-IL-FeTPPS was estimated to be 4.2 μmol g^{-1}.

The morphology of Fe_3O_4, Fe_3O_4@SiO_2-IL and Fe_3O_4@SiO_2-IL-FeTPPS microspheres was examined from SEM images. The SEM image, shown in Fig. S1, suggested that the particles formed sphere-like shapes. These microspheres appeared to be well-distributed with an average diameter about 300 nm. TEM images of Fe_3O_4, Fe_3O_4@SiO_2-IL and Fe_3O_4@SiO_2-IL-FeTPPS are shown in Fig. S2. The thickness of the coated layer was estimated to be around 5–10 nm.

The XRD patterns in Fig. S3 showed that the diffraction peaks for the Fe_3O_4@SiO_2-IL-FeTPPS and Fe_3O_4 microspheres had similar locations, in good agreement with the XRD pattern for Fe_3O_4 in a previous report [32], in which the synthesized Fe_3O_4@SiO_2-IL-FeTPPS microspheres were reported to have the same crystal structure as naked Fe_3O_4 particles. The EDX spectra of Fe_3O_4@SiO_2 and Fe_3O_4@SiO_2-IL microspheres confirm the successful functionalization of the coating of the silica layer and the IL on the magnetic core. The strong silica peak appeared in the TEM-EDX spectrum of Fe_3O_4@SiO_2 (Fig. 1a) and a chlorine peak (Fig. 1b), which was likely derived from a counter anion of IL, was clearly visible in the TEM-EDX spectrum of the Fe_3O_4@SiO_2-IL. In addition, the Fe signal in the XPS spectrum of Fe_3O_4@SiO_2-IL had disappeared, compared with naked Fe_3O_4 (Fig. S4). These results suggest that the Fe_3O_4 surfaces were successfully coated with silica and IL.

Changes in the surface chemistry of the Fe_3O_4, Fe_3O_4@SiO_2-IL and Fe_3O_4@SiO_2-IL-FeTPPS were characterized from zeta potential data, which is related to the surface charge (Fig. 2). Unmodified Fe_3O_4 had a positive surface charge at pH values below 4.6 and a negative charge at pH values higher than 4.6 due to the dissociation of acidic surface hydroxyl groups. The point of zero charge (PZC) of Fe_3O_4@SiO_2-IL shifted to lower a pH value at 3.7, consistent with IL being modified on the Fe_3O_4@SiO_2 surface. The PZC for Fe_3O_4@SiO_2-IL-FeTPPS was pH 4.7, similar to that for Fe_3O_4. This suggests that surface functionalization of Fe_3O_4 did not dramatically alter the types of basic and acidic groups associated with the Fe_3O_4 because of relatively lower loading amount of FeTPPS (4.2 μmol g^{-1}). The higher negative zeta potential values above pH 4.7 indicate that the Fe_3O_4@SiO_2-IL-FeTPPS carried a larger amount of negative charge, compared to Fe_3O_4 and Fe_3O_4@SiO_2-IL. The higher charges of Fe_3O_4@SiO_2-IL-FeTPPS may be due to the generation of more amphoteric sites by the FeTPPS as an anionic porphyrin and by coating with silica. The higher negative surface charge would be expected to inhibit the agglomeration of the catalyst and the

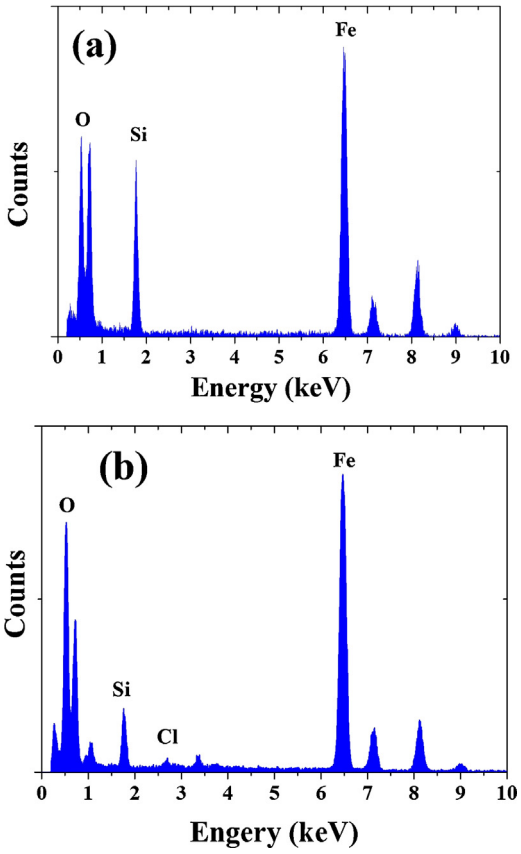

Fig. 1. TEM-EDX spectra of Fe_3O_4@SiO_2 (a) and Fe_3O_4@SiO_2-IL (b).

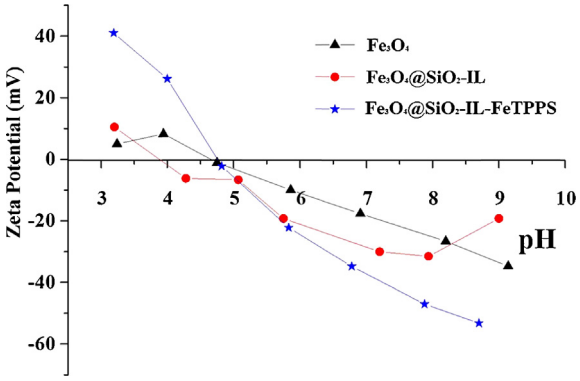

Fig. 2. The pH dependence on the zeta potential for Fe_3O_4, Fe_3O_4@SiO_2-IL, and Fe_3O_4@SiO_2-IL-FeTPPS.

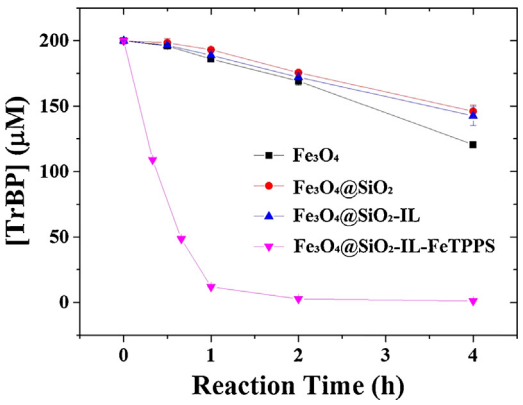

Fig. 4. Influence of catalyst type on the TrBP degradation. The reaction conditions were as follows: [catalysts] 1 g L^{-1}, $[KHSO_5]_0$ 500 μM, $[TrBP]_0$ 200 μM, and pH 6.

adsorption of phenolic compounds and other degradation products, which can contribute to maintaining a high catalytic activity during the reaction.

Fig. 3 shows Fourier transform infrared (FT-IR) spectra of both the unfunctionalized and functionalized Fe_3O_4 samples. The Fe—O stretching vibration near 583 cm^{-1} and the O—H stretching vibration near 3304 cm^{-1} were observed in Fe_3O_4, Fe_3O_4@SiO_2, Fe_3O_4@SiO_2-IL and Fe_3O_4@SiO_2-IL-FeTPPS. Typical bands associated with stretching, bending, and out-of-plane deformation vibrations of Si—O—Si bonds at 1082 and 1235 cm^{-1} were observed in Fe_3O_4@SiO_2, Fe_3O_4@SiO_2-IL and Fe_3O_4@SiO_2-IL-FeTPPS. The FT-IR spectrum of Fe_3O_4@SiO_2-IL included characteristic vibration bands at around 2976 cm^{-1}, which correspond to symmetrical and asymmetrical C—H stretching vibrations of the methyl group in IL. The peak at 3016 cm^{-1} is assigned to C—H (C=C, sp^2) and the weak absorption bands at 1400–1600 cm^{-1} to C=C, C=N ring stretching of the imidazole ring (skeletal bands) were present in the spectra of Fe_3O_4@SiO_2-IL. The appearance of these bands confirms that IL is introduced in the Fe_3O_4@SiO_2-IL. An increase in the absorption at 1132 cm^{-1} in the spectra of Fe_3O_4@SiO_2-IL-FeTPPS, which corresponds to the symmetrical and asymmetrical S=O stretching vibrations of the sulfonatephenyl group in FeTPPS, provides support for the conclusion that the FeTPPS is loaded in the Fe_3O_4@SiO_2-IL.

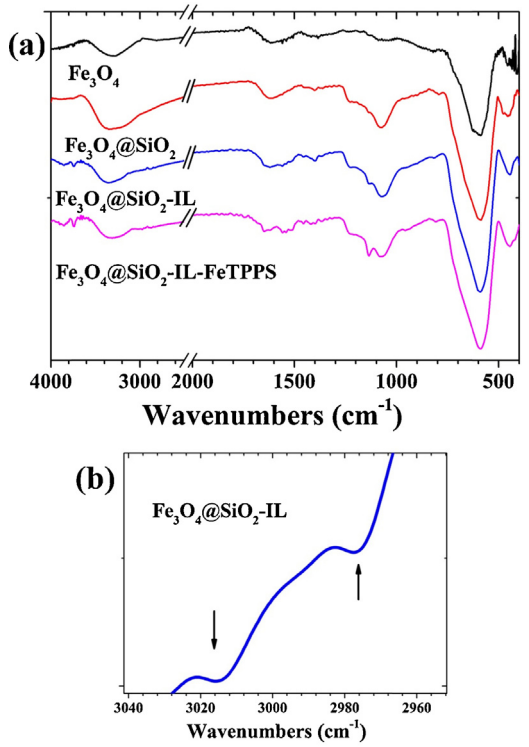

Fig. 3. FT-IR spectra of Fe_3O_4, Fe_3O_4@SiO_2, Fe_3O_4@SiO_2-IL, and Fe_3O_4@SiO_2-IL-FeTPPS samples (a) and a partial FT-IR spectrum of Fe_3O_4@SiO_2-IL in the range of 3040–2050 cm^{-1} (b).

3.2. Comparison of catalytic activities for Fe_3O_4, Fe_3O_4@SiO_2, Fe_3O_4@SiO_2-IL and Fe_3O_4@SiO_2-IL-FeTPPS

The catalytic activities of Fe_3O_4, Fe_3O_4@SiO_2, Fe_3O_4@SiO_2-IL and Fe_3O_4@SiO_2-IL-FeTPPS were investigated for a $[KHSO_5]_0/[TrBP]_0 = 2.5$ (Fig. 4). The initial concentrations of TrBP and $KHSO_5$ were set at 200 μM and 500 μM, respectively. Although the naked Fe_3O_4 showed catalytic activity for the degradation of TrBP, around 40% of the TrBP was degraded within 4 h. As shown in the ESR spectra (Fig. 5), in the presence of $KHSO_5$ and Fe_3O_4, a nine-line peak in the ESR spectrum with hyperfine splitting constants of $A_N = 7.2$ G and A_H (2H) = 4.2 G were observed, which was identified as DMPOX (5,5-dimethyl-2-oxo-pyrroline-1-oxyl), as assigned previously [36]. The DMPOX signal disappeared after 18 min and peaks corresponding to •DMPO-HO then appeared in the presence of Fe_3O_4 (Fig. 5). The activation of $KHSO_5$ may produce sulfate, peroxy-sulfate and hydroxyl radicals [37]. Hydroxyl radicals may be generated by the reaction of sulfate radical with

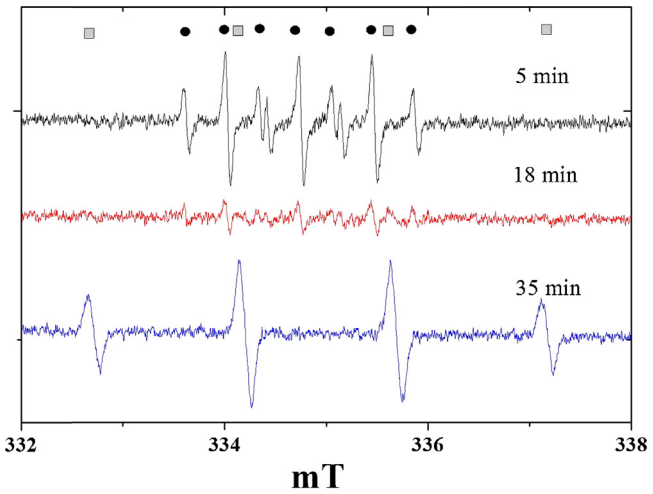

Fig. 5. ESR spectra of aqueous mixture for Fe_3O_4, $KHSO_5$ and DMPO at different reaction period after adding $KHSO_5$. Reaction conditions: $[Fe_3O_4]$ 1 g L^{-1}, $[KHSO_5]_0$ 500 μM, pH 6, and [DMPO] 0.1 M.

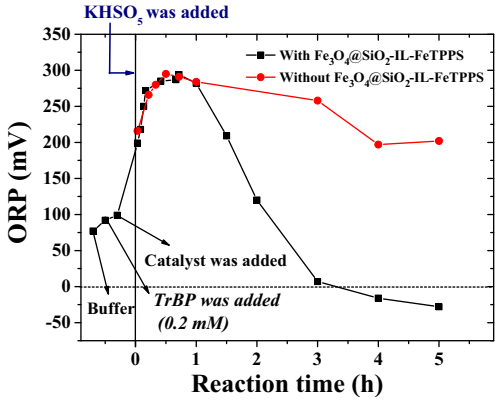

Fig. 6. The variations in ORP during the degradation of TrBP. Reaction conditions: $[TrBP]_0$ 200 μM, $[KHSO_5]_0$ 0.5 mM, pH 6 and $[Fe_3O_4@SiO_2\text{-IL-FeTPPS}]$ 1 g L^{-1}.

H_2O [37]. To identify the major reactive species generated in the $Fe_3O_4/KHSO_5$ system, alcohols were added to reaction solution as quenching agents. Ethanol reacts with $HO^•$ and $SO_4^{•-}$ at high and comparable rates [38]. However, tert-butyl alcohol (TBA) reacts with $HO^•$ faster than with $SO_4^{•-}$ [38]. As shown in Fig. S5, when no quenching agents were added, about 40% of the TrBP was degraded in 4 h. However, the addition of 0.1 M TBA and 0.1 M ethanol (EtOH) resulted in a decreased TrBP removal (4 h) to 36% and 17%, respectively. The much larger decrease in the removal of TrBP in the presence of EtOH than by TBA suggests that the main radical species generated during the activation of $KHSO_5$ by Fe_3O_4 were sulfate radicals. However, due to the lower sensitivity and short lifetime of •DMPO-SO_4^-, a signal for •DMPO-SO_4^- was not detected [39]. These results suggest that $SO_4^{•-}$ is a critical factor in the degradation of TrBP using the $Fe_3O_4/KHSO_5$ system.

For $Fe_3O_4@SiO_2$ and $Fe_3O_4@SiO_2$-IL, some degradation of TrBP was observed. The intensity of the •DMPO-HO peaks remarkably decreased in the $Fe_3O_4@SiO_2$-IL/$KHSO_5$ system (Fig. S6a). This suggests that the surface ferrous ions of Fe_3O_4 play a key role in the generation of $SO_4^{•-}$.

As shown in Fig. 4, $Fe_3O_4@SiO_2$-IL-FeTPPS significantly enhanced the catalytic oxidation of TrBP (TOF, 54.1 h^{-1} at 0.67 h of period). However, except for the DMPOX peak at 5 min, no other radical species were observed (Fig. S6b). The enhanced catalytic activities for the $Fe_3O_4@SiO_2$-IL-FeTPPS may be due to oxo-ferryl porphyrin species derived from the conventional peroxidase shunt pathway [8,16] but this does not account for the production of $SO_4^{•-}$. The catalytic activity for degradation kinetics in the homogeneous iron(III)-porphyrin system is higher than that in the heterogeneous system, as described in previous reports [12]. Thus, the higher catalytic activity in the $Fe_3O_4@SiO_2$-IL-FeTPPS/$KHSO_5$ system may be due to the stabilization of the FeTPPS catalyst in the IL phase and the restoration of homogeneous conditions on the surface of the Fe_3O_4.

Because $KHSO_5$ is a strong oxidant, the oxidation reduction potentials (ORPs) in the reaction mixture were measured, and the results are shown in Fig. 6. The ORPs of the buffer, 0.2 mM TrBP buffer and 0.2 mM TrBP buffer solutions with 1 g L^{-1} of the $Fe_3O_4@SiO_2$-IL-FeTPPS catalyst were in the range of 50–100 mV. The ORP increased to over 200 mV within 2 min after adding the $KHSO_5$ in both the presence and absence of catalyst. In the $Fe_3O_4@SiO_2$-IL-FeTPPS/$KHSO_5$ catalytic system, the higher level of ORP was maintained for 1 h and then dropped sharply from +282 mV to −28 mV for the remaining 1–5 h of the reaction period. This indicates that the $KHSO_5$ was consumed by the oxidation reaction. In contrast, in the absence of the catalyst, the ORP in the presence of $KHSO_5$ alone remained relatively constant for a period

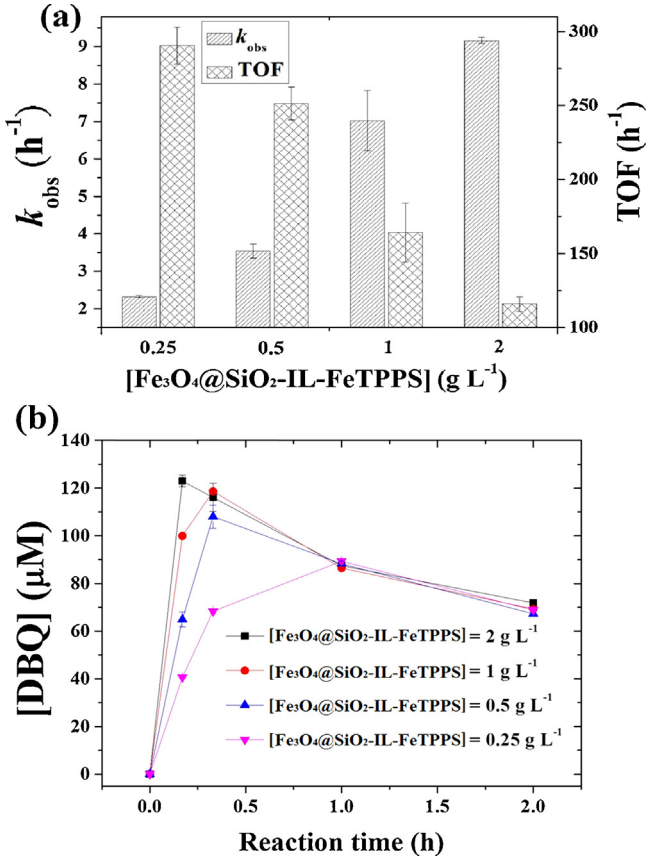

Fig. 7. Influence of catalyst dosage on the TrBP degradation (a) and DBQ concentration (b). Reaction conditions: $[Fe_3O_4@SiO_2\text{-IL-FeTPPS}]$ 1 g L^{-1}, $[KHSO_5]_0$ 1 mM, $[TrBP]_0$ 200 μM, and pH 6.

of 3 h, and then decreased slightly after 4 h. Because no TrBP degradation was observed for the 4 h of period, it can be assumed that no oxidation–reduction reactions occurred.

3.3. Influence of catalyst dosage on the TrBP degradation

Fig. 7 shows the influence of catalyst concentration on TrBP degradation and on the main degradation intermediate, 2,6-dibromo-*p*-benzoquinone (DBQ). The pseudo-first-order rate constant for the degradation of TrBP increased with increasing catalyst concentration (Fig. 7a). However, the TOF decreased with increasing catalyst concentration. In the presence of 1 and 2 g L^{-1} $Fe_3O_4@SiO_2$-IL-FeTPPS, approximately 100% of the TrBP was degraded within 30 min. Fig. 7b shows the kinetics of DBQ formation as a result of the oxidation of TrBP. The DBQ initially increased and then gradually decreased. However, the maximum value and the initial rate for the formation of DBQ increased with increasing $Fe_3O_4@SiO_2$-IL-FeTPPS concentration. The reaction time for the highest DBQ level was retarded and the highest DBQ concentration decreased with decreasing catalyst dosage. After the reaching the maximum value, the DBQ concentration decreased gradually, accompanied by the further degradation of DBQ via the oxidation with the $Fe_3O_4@SiO_2$-IL-FeTPPS/$KHSO_5$ catalytic system. Catalyst reusability is an important factor in the evaluation of catalyst stability. The reusability of $Fe_3O_4@SiO_2$-IL-FeTPPS was investigated at pH 6. The percent of TrBP degradation remained constant after 3 recyclings (Fig. S7). To evaluate the stability of Fe_3O_4 and $Fe_3O_4@SiO_2$-IL-FeTPPS, the leaching of iron was measured after 4 h period of TrBP degradation with 1 g L^{-1} of catalyst. An ICP-AES analysis indicated that the leaching of iron was about

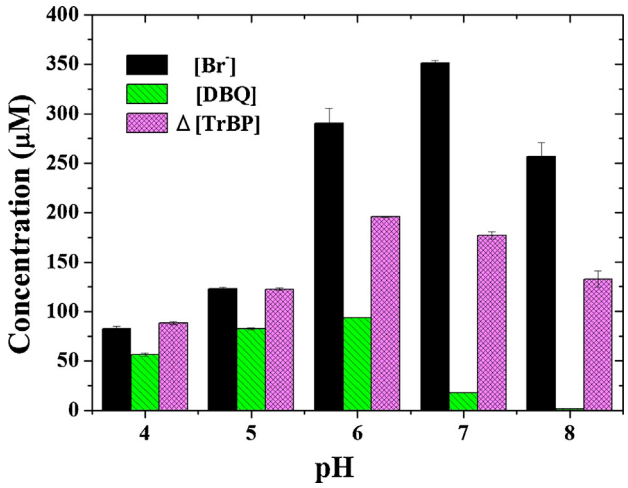

Fig. 8. Influence of pH on the TrBP degradation, DBQ formation and released Br^-. Reaction conditions: [Fe_3O_4@SiO_2-IL-FeTPPS] 1 g L^{-1}, [$KHSO_5$]$_0$ 500 μM, [TrBP]$_0$ 200 μM, and reaction period 2 h.

40 μg L^{-1} in the Fe_3O_4/$KHSO_5$ system, while less than 10 μg L^{-1} was found in the case of the Fe_3O_4@SiO_2-IL-FeTPPS/$KHSO_5$.

3.4. Influence of pH on the TrBP degradation

Because the redox potentials of $KHSO_5$, TrBP and other dissolved species are pH dependent, the influence of pH on the oxidative degradation of TrBP was investigated after a 2 h incubation period. Fig. 8 illustrates the effect of pH on TrBP degradation, the formation of a major oxidation product, DBQ, and the released Br^-. Concentrations of the degraded TrBP (Δ[TrBP]) and DBQ ([DBQ]) increased with an increase in pH, reaching a maximum at pH 6, and then decreased at pH values above 6. At pH 4 and 5, the [DBQ] was slightly lower than the Δ[TrBP] and the released [Br^-] was almost the same as the level of the Δ[TrBP]. These results show that the degraded TrBP is nearly completely transformed into DBQ and one Br atom is released into the solution. From pH 6–8, the Δ[TrBP] and the level of released [Br^-] increased, compared to a lower pH range, and 100% of the TrBP was degraded at pH 6.

3.5. Influence of HA dosage on TrBP degradation

HAs are a major component of landfill leachates, and play a key role in the leaching, transition and degradation of organic pollutants [40]. It has been reported that HAs function as inhibitors of the degradation of bromophenols [14,15,41]. The inhibition of HA is mainly caused by competition for oxidative species, because HAs contain large amounts of quinines and phenolic moieties and the inhibition occurs via interactions of substrates and/or catalysts due to the colloidal heterogeneous properties of HAs [12,42]. Thus, the influence of HAs on TrBP degradation was investigated in the pH range from 4 to 8 in the presence of 25 mg L^{-1} HA, as summarized in Table 1. The $\Delta[TrBP]_{HA}$ and Δ[TrBP] in Table 1 represent the concentrations of degraded TrBP in the presence and absence of HA (25 mg L^{-1}), respectively. Values lower than 1 indicate the inhibition of TrBP degradation by HA. The degradation of TrBP was not inhibited at pH 4–6, while inhibition was observed at pH 7 and 8. As shown in Fig. 8, the formation of the major byproduct, DBQ, indicated a maximum value at pH 6, in which DBQ formation was slightly inhibited. Debromination was slightly inhibited in the presence of HA at pH 4, 6 and 7, while substantial inhibition by HA was observed at pH 8.

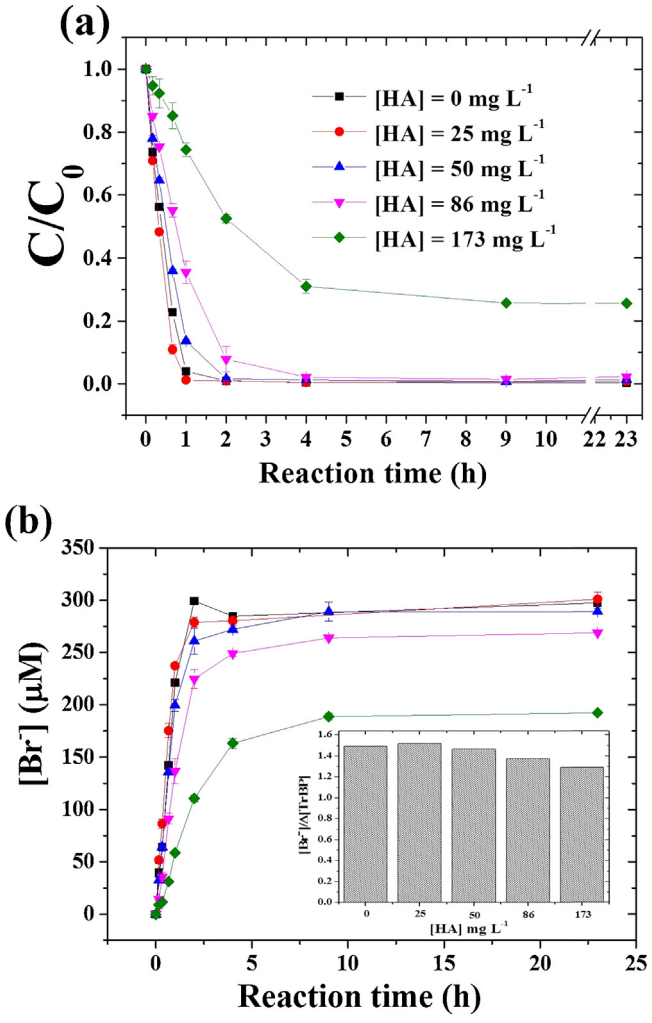

Fig. 9. Influence of HA concentration on the TrBP degradation (a) and debromination (b). Reaction conditions: [Fe_3O_4@SiO_2-IL-FeTPPS] 1 g L^{-1}, [$KHSO_5$]$_0$ 0.5 mM, [TrBP]$_0$ 200 μM, and pH 6.

Because of the highest Δ[TrBP], the influences of HA concentration on the kinetics of degradation and debromination were investigated at pH 6 (Fig. 9). Table 2 summarizes the TOF values and pseudo-first-order rate constants (k_{obs}). The TOF values and k_{obs} were relatively constant in the presence of 0–50 mg L^{-1} HA.

Table 1
Influence of HA on the concentration of degraded TrBP, DBQ and released Br^-.[a]

pH	$\Delta[TrBP]_{HA}$ (μM)[b]	$\frac{\Delta[TrBP]_{HA}}{\Delta[TrBP]}$	$[DBQ]_{HA}$ (μM)	$\frac{[DBQ]_{HA}}{[DBQ]}$	$[Br^-]_{HA}/\Delta[TrBP]_{HA}$	$\frac{[Br^-]_{HA}/\Delta[TrBP]_{HA}}{[Br^-]/\Delta[TrBP]}$
4	88.5	1.00	76.9	1.36	0.87	0.93
5	156.2	1.27	118.9	1.44	0.84	0.84
6	196.3	1.00	91.3	0.97	1.40	0.94
7	159.8	0.90	13.9	0.78	1.89	0.95
8	97.7	0.74	0.0	0.00	1.44	0.74

[a] Reaction conditions: [Fe_3O_4@SiO_2-IL-FeTPPS] 1 g L^{-1}, [$KHSO_5$]$_0$ 0.5 mM, [TrBP]$_0$ 200 μM, [HA] 25 mg L^{-1}, reaction time 2 h.
[b] The concentration of degraded TrBP

Table 2
Influence of HA concentration on TOF and k_{obs} for TrBP degradation.[a]

[HA] (mg L^{-1})	k_{obs} (h^{-1})[b]	TOF (h^{-1})[c]	
		TrBP	Br^-
0	2.5	62.6	45.8
25	2.8	73.8	61.9
50	2.0	50.4	46.0
86	1.2	35.2	25.5
173	0.3	11.0	8.3

[a] Reaction conditions: [Fe_3O_4@SiO_2-IL-FeTPPS] 1 g L^{-1}, [$KHSO_5$]$_0$ 0.5 mM, [TrBP]$_0$ 200 μM, [HA] 25 mg L^{-1}, pH 6.
[b] Pseudo first-order rate constant.
[c] Turnover frequencies (TOFs) were calculated by dividing the rate of degradation of TrBP (μM h^{-1}) or the rate of debromination at 0.33 h of reaction period by the concentration of the catalyst (4.2 μM).

However, the presence of 173 mg L^{-1} HA resulted in the significant inhibition of the degradation and debromination of TrBP. For the case of iron(III)-porphyrins supported on the silica surface and mesoporous silica [12–14], only 25 mg L^{-1} of HA led to a significant inhibition of bromophenol oxidation. Thus, Fe_3O_4@SiO_2-IL-FeTPPS is effective in eliminating the inhibition of TrBP degradation in the presence of HA.

3.6. The mineralization of TrBP

As shown in Fig. 7b, DBQ degraded after its formation at the initial stage of the oxidation reaction. The oxidative degradation of a quinone leads to the formation of organic acids via ring-cleavage and then mineralization to CO_2 [43]. There are a few reports on the mineralization of chlorophenols by iron(III)-porphyrins/$KHSO_5$ catalytic systems [8,21]. However, in the iron(III)-porphyrin/$KHSO_5$ system, the oxidation of bromophenol is more difficult than those of fluoro- and chlorophenols [44]. Thus, mineralization was examined by the analysis of total organic carbon (TOC) in a reaction mixture at pH 6. To achieve the mineralization of TrBP, the reaction was examined when $KHSO_5$ was sequentially added at 24 h intervals (↓ in Fig. 10a and b). In the first 24 h of the reaction, 15% of the TrBP was mineralized when the Fe_3O_4@SiO_2-IL-FeTPPS catalyst was used. Even though the debromination was observed with Fe_3O_4, no mineralization was detected. After two additions of $KHSO_5$, the mineralization of TrBP significantly increased to 48% in the presence of Fe_3O_4@SiO_2-IL-FeTPPS catalyst. In the same time, the percent mineralization with Fe_3O_4 was increased to 17%. The highest mineralization (55%) was achieved after adding 3 portions of $KHSO_5$ with the Fe_3O_4@SiO_2-IL-FeTPPS catalyst. The percent mineralization of TrBP with Fe_3O_4@SiO_2-IL, which is a precursor of Fe_3O_4@SiO_2-IL-FeTPPS, was slightly higher than that in the presence of Fe_3O_4 (Fig. S8). Because the zeta potential for Fe_3O_4 indicates that it has a relatively less negative surface charge than that Fe_3O_4@SiO_2-IL (Fig. 2), the deactivation of Fe_3O_4 due to catalyst agglomeration and the adsorption of phenolic compounds and other degradation products may be responsible for the observed lower mineralization. The mineralization of TrBP in the Fe_3O_4@SiO_2-IL-FeTPPS/$KHSO_5$ system was monitored by UV–vis absorption spectra (Fig. S9). The absorption peaks for TrBP at 210 nm, 250 nm and 318 nm disappeared, indicative of the degradation of TrBP. Moreover, as the reaction proceeded, the intensity of an absorption corresponding to a π–π* transition of an aromatic ring in DBQ at 200–220 nm and 290 nm in the UV region also decreased, suggesting that DBQ was decomposed and that TrBP had been mineralized. The concentrations of the released Br^- are shown in Fig. 10b. Debromination decreased slightly with the addition of $KHSO_5$ in the Fe_3O_4/$KHSO_5$ system. In the Fe_3O_4@SiO_2-IL-FeTPPS/$KHSO_5$ system, the debromination decreased slightly after the second addition, and 43% of the debromination was achieved after the third addition. The decrease in debromination by sequentially adding $KHSO_5$ can be attributed to the oxidation of Br^- [14].

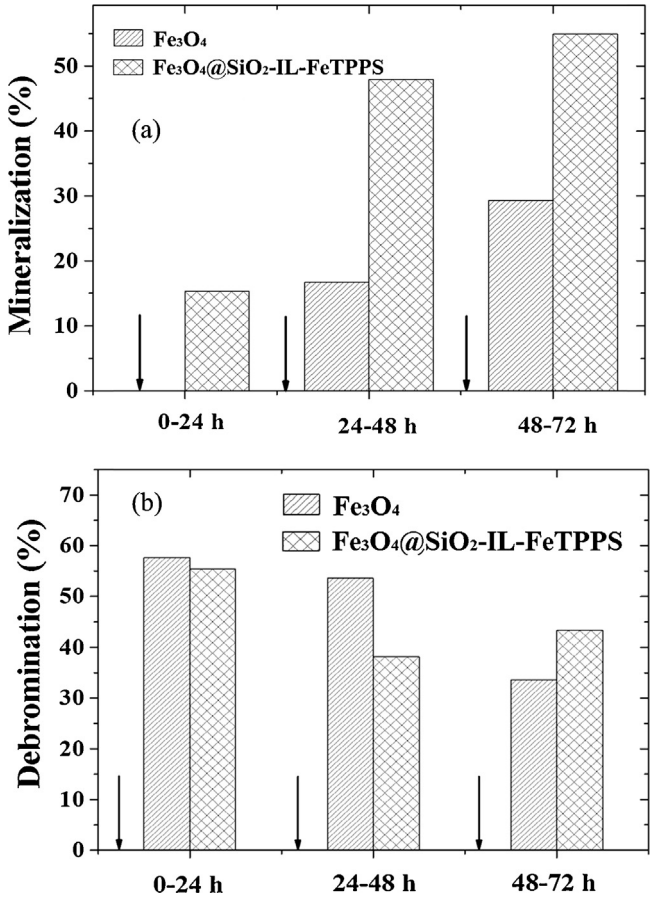

Fig. 10. The variations in the percent mineralization (a) and debromination (b) at pH 6 by the sequential addition of $KHSO_5$ after a 24 h period. Reaction conditions: [TrBP]$_0$ 200 μM, [$KHSO_5$]$_0$ 1 mM, and [Fe_3O_4@SiO_2-IL-FeTPPS] 1 g L^{-1}.

4. Conclusion

The Fe_3O_4@SiO_2-IL-FeTPPS catalyst was found to be effective for TrBP degradation at pH 6. Although the major oxidation product was DBQ, it also disappeared further, suggesting the occurrence of mineralization. 55% of the TrBP was mineralized with the Fe_3O_4@SiO_2-IL-FeTPPS catalyst. The presence of HA, a major component in leachates, has usually an adverse effect on the oxidation of TrBP. However, no significant decrease in catalytic activity for TrBP degradation was observed in the presence of 86 mg L^{-1} HA for the Fe_3O_4@SiO_2-IL-FeTPPS/$KHSO_5$ catalytic system. The higher catalytic activity of the Fe_3O_4@SiO_2-IL-FeTPPS catalyst can be attributed to the fact that the IL modified surface plays an important role in restoring homogeneous catalytic efficiency to the supported FeTPPS.

Acknowledgment

This work was supported by Grants-in-Aid for Scientific Research from Japan Society for Promotion of Science (25241017).

Appendix A. Supplementary data

Supplementary data associated with this article can be found, in the online version, at http://dx.doi.org/10.1016/j.apcatb.2014.08.035.

References

[1] R.J. Law, C.R. Allchin, J. de Boer, A. Covaci, D. Herzke, P. Lepom, S. Morris, J. Tronczynski, C.A. de Wit, Chemosphere 64 (2006) 187–208.
[2] W.-J. Sim, S.-H. Lee, I.-S. Lee, S.-D. Choi, J.-E. Oh, Chemosphere 77 (2009) 552–558.
[3] P.D. Howe, S. Dobson, H.M. Malcolm, 2,4,6-Tribromophenol and Other Simple Brominated Phenol, World Health Organization, Geneva, 2005.
[4] EPA, Organobromine Production Wastes; Identification and Listing of Hazardous Waste; Land Disposal Restrictions; Listing of CERCLA Hazardous Substances, Reportable Quantitiestle, USA, 1998.
[5] I.A.T. Meerts, J.J. van Zanden, E.A. Luijks, I. van Leeuwen-Bol, G. Marsh, E. Jakobsson, A. Bergman, A. Brouwer, Toxicol. Sci. 56 (2000) 95–104.
[6] K.-I. Choi, S.-H. Lee, M. Osako, Chemosphere 74 (2009) 460–466.
[7] M. Osako, Y.-J. Kim, S. Sakai, Chemosphere 57 (2004) 1571–1579.
[8] M. Fukushima, K. Tatsumi, Environ. Sci. Technol. 39 (2005) 9337–9342.
[9] K.C. Christoforidis, M. Louloudi, E.R. Milaeva, Y. Deligiannakis, J. Catal. 270 (2010) 153–162.
[10] M. Fukushima, J. Mol. Catal. A: Chem. 286 (2008) 47–54.
[11] S. Shigetatsu, M. Fukushima, S. Nagao, J. Environ. Sci. Heal. A 45 (2010) 1536–1542.
[12] Q. Zhu, S. Maeno, R. Nishimoto, T. Miyamoto, M. Fukushima, J. Mol. Catal. A: Chem. 385 (2014) 31–37.
[13] Q. Zhu, Y. Mizutani, S. Maeno, M. Fukushima, Molecules 18 (2013) 5360–5372.
[14] Q. Zhu, Y. Mizutani, S. Maeno, R. Nishimoto, T. Miyamoto, M. Fukushima, J. Environ. Sci. Heal. A 48 (2013) 1593–1601.
[15] M. Fukushima, H. Ichikawa, M. Kawasaki, A. Sawada, K. Morimoto, K. Tatsumi, Environ. Sci. Technol. 37 (2003) 386–394.
[16] M. Fukushima, A. Sawada, M. Kawasaki, H. Ichikawa, K. Morimoto, K. Tatsumi, M. Aoyama, Environ. Sci. Technol. 37 (2003) 1031–1036.
[17] M. Fukushima, Y. Tanabe, K. Morimoto, K. Tatsumi, Biomacromolecules 8 (2007) 386–391.
[18] K.C. Christoforidis, E. Serestatidou, M. Louloudi, I.K. Konstantinou, E.R. Milaeva, Y. Deligiannakis, Appl. Catal. B: Environ. 101 (2011) 417–424.
[19] K.C. Christoforidis, M. Louloudi, Y. Deligiannakis, Appl. Catal. B: Environ. 95 (2010) 297–302.
[20] G. Díaz-Díaz, M. Celis-García, M.C. Blanco-López, M.J. Lobo-Castañón, A.J. Miranda-Ordieres, P. Tuñón-Blanco, Appl. Catal. B: Environ. 96 (2010) 51–56.
[21] M. Fukushima, S. Shigematsu, J. Mol. Catal. A: Chem. 293 (2008) 103–109.
[22] M. Fukushima, K. Tatsumi, J. Mol. Catal. A: Chem. 245 (2006) 178–184.
[23] T. Miyamoto, R. Nishimoto, S. Maeno, Q. Zhu, M. Fukushima, J. Mol. Catal. B: Enzym. 99 (2014) 150–155.
[24] T. Fukushima, T. Aida, Chem. Eur. J. 13 (2007) 5048–5058.
[25] J.L. Kaar, A.M. Jesionowski, J.A. Berberich, R. Moulton, A.J. Russell, J. Am. Chem. Soc. 125 (2003) 4125–4131.
[26] W. Miao, T.H. Chan, Acc. Chem. Res. 39 (2006) 897–908.
[27] N.M.T. Lourenço, S. Barreiros, C.A.M. Afonso, Green Chem. 9 (2007) 734–736.
[28] J. Łuczak, J. Hupka, J. Thöming, C. Jungnickel, Colloid Surf. A 329 (2008) 125–133.
[29] M. Smiglak, A. Metlen, R.D. Rogers, Acc. Chem. Res. 40 (2007) 1182–1192.
[30] R. Šebesta, I. Kmentová, Š. Toma, Green Chem. 10 (2008) 484–496.
[31] X. Ma, Y. Zhou, J. Zhang, A. Zhu, T. Jiang, B. Han, Green Chem. 10 (2008) 59–66.
[32] Z. Zhang, F. Zhang, Q. Zhu, W. Zhao, B. Ma, Y. Ding, J. Colloid Interface Sci. 360 (2011) 189–194.
[33] F. Tanaka, M. Fukushima, A. Kikuchi, H. Yabuta, H. Ichikawa, K. Tatsumi, Chemosphere 58 (2005) 1319–1326.
[34] M. Kawasaki, A. Kuriss, M. Fukushima, A. Sawada, K. Tatsumi, J. Porphyr. Phthalocya. 7 (2003) 645–650.
[35] H. Yang, X. Han, G. Li, Y. Wang, Green Chem. 11 (2009) 1184–1193.
[36] T. Ozawa, Y. Miura, J.-I. Ueda, Free Radic. Biol. Med. 20 (1996) 837–841.
[37] M. Pagano, A. Volpe, G. Mascolo, A. Lopez, V. Locaputo, R. Ciannarella, Chemosphere 86 (2012) 329–334.
[38] Y. Ding, L. Zhu, N. Wang, H. Tang, Appl. Catal. B: Environ. 129 (2013) 153–162.
[39] K. Ranguelova, A.B. Rice, A. Khajo, M. Triquigneaux, S. Garantziotis, R.S. Magliozzo, R.P. Mason, Free Radic. Biol. Med. 52 (2012) 1264–1271.
[40] M. Hofrichter, A. Steinbüchel (Eds.), Biopolymer, Wiley-VCH, Weinheim, Germany, 2001.
[41] J. Ma, N.J.D. Graham, Water Res. 33 (1999) 785–793.
[42] M. Aeschbacher, C. Graf, R.P. Schwarzenbach, M. Sander, Environ. Sci. Technol. 46 (2012) 4916–4925.
[43] R. Vinu, S. Polisetti, G. Madras, Chem. Eng. J. 165 (2010) 784–797.
[44] M. Fukushima, Y. Mizutani, S. Maeno, Q. Zhu, H. Kuramitz, S. Nagao, Molecules 17 (2011) 48–60.